Journal of
Computational and Theoretical Nanoscience
Vol. 2, 45–55, 2005

Design and Analysis of a Molecular Tool for Carbon Transfer in Mechanosynthesis

Damian G. Allis[1] and K. Eric Drexler[2,*]

[1] Syracuse University, Center for Science and Technology, Syracuse, NY 13224, USA
[2] Foresight Institute, 1455 Adams Drive, Menlo Park, CA 94025, USA

Mechanosynthesis of a target class of graphene-, nanotube-, and diamond-like structures will require molecular tools capable of transferring carbon moieties to structures that have binding energies in the range of 1.105 to 1.181 aJ per atom (159 to 170 kcal mol^{-1}). Desirable properties for tools include exoergic transfer of moieties to these structures; good geometrical exposure of moieties; and structural, electronic, and positional stability. We introduce a novel carbon-transfer tool design (named by us "DC10c"), the first predicted to exhibit these properties in combination. The DC10c tool is a stiff hydrocarbon structure that binds carbon dimers through strained σ-bonds. On dimer removal, diradical generation at the dimer-binding sites is avoided by means of π-delocalization across the binding face of the empty form, creating a strained aromatic ring. Transfer of carbon dimers to each of the structures in the target class is exoergic by a mean energy >0.261 aJ per dimer (>38 kcal mol^{-1}); this is compatible with transfer-failure rates of $\sim 10^{-24}$ per operation at 300 K. We present a B3LYP/6-31G(d,p) study of the geometry and energetics of DC10c, together with discussion of its anticipated reliability in mechanosynthetic applications.

Keywords: Quantum Chemistry, Mechanosynthesis, Graphene, Graphite, Diamond, Nanotube, Productive Nanosystems, Molecular Manufacturing, Nanotechnology.

1. INTRODUCTION

Mechanosynthesis exploits mechanical positioning to direct reactive moieties to specific reactive sites on target structures. This mechanism of control contrasts with that of conventional synthesis techniques, in which solution-phase diffusion produces undirected molecular encounters. Despite this lack of direct positional control, diffusion-based synthesis techniques can achieve considerable site specificity by seeking reaction sequences in which each distinct reactive site, at each step, differs from the rest in its reactivity. This strategy for structural control becomes more difficult as structures grow larger and more complex, due to the proliferation of similar reactive sites. Mechanosynthetic techniques, in contrast, can perform different synthetic operations on target sites of similar reactivity that are distinguished solely by their structural position. This means of control is essentially independent of product scale and complexity and can be quite reliable. Diffusion-based synthesis techniques have been under development for more than a century and have achieved striking results. Mechanosynthetic techniques are rudimentary today, but their further development promises to greatly expand the scale, diversity, and complexity of products made by structurally precise molecular synthesis.

The following discussion addresses operations suitable for an advanced class of mechanosynthetic systems that work in a "machine phase" characterized by strict constraints on the motions and encounter geometries of *all* reactive moieties involved. This entails rigorous exclusion of unconstrained molecules. In this regard, the machine phase resembles the "inner phase" of molecular containers;[1] they are similar in their ability to stabilize a range of structures that would otherwise essentially behave as short-lived reactive intermediates. The dynamical behavior of molecules in a machine-phase system is qualitatively different from that of the immobile or diffusing molecules found in solid-, liquid-, and gas-phase systems, or at their interfaces. (Mechanosynthesis is, of course, not synonymous with advanced machine-phase

*Author to whom correspondence should be addressed.

 1546-198X/2005/2/045/011/$17.00+.25 doi:10.1166/jctn.2005.003

systems: mechanosynthetic operations *in vacuo,* some aided by electron flow, have been demonstrated experimentally,[2–5] and mechanosynthetic operations in a solvent also appear feasible, using conventional reactants bound to modified scanning-probe tips.[6, 7])

Machine-phase systems have several advantages, both in anticipated practice and in current theoretical studies. When implemented, these systems will enable the use of reactive, high-energy molecular species in a well-controlled manner, avoiding most unwanted reactions by preventing unwanted molecular encounters. These advantages, in turn, promise to expand the range of feasible products to include a range of strong covalent solids with bonding properties like those found in graphite, diamond, and crystalline silicon, including intricate structures unlike any that can be made today. Finally, these systems lend themselves to computational modeling, both because strict motion constraints reduce the number of configurations that must be examined, and because reactions that consume high-energy species can have large thermodynamic driving forces, making predicted behaviors relatively insensitive to errors in calculated model energies. Design studies of machine-phase mechanosynthetic systems have been presented in several publications,[8–14] as have suggested multi-stage development strategies leading toward their implementation.[8, 9, 14–17]

2. THE DC10c DESIGN

This paper presents a density functional theory (DFT) study of a novel reactive tool structure (called "DC10c;" Fig. 1) suitable for transferring carbon dimers to specific sites in graphene- and diamond-like structures. It is a high-energy hydrocarbon structure, containing strained and unsaturated bonds. Other structures and reactions for use in machine-phase mechanosynthesis (including tools for carbon dimer placement and for hydrogen removal to produce reactive sites) have been proposed[8, 18, 20] and analyzed[18–21] using *ab initio* and DFT methods.

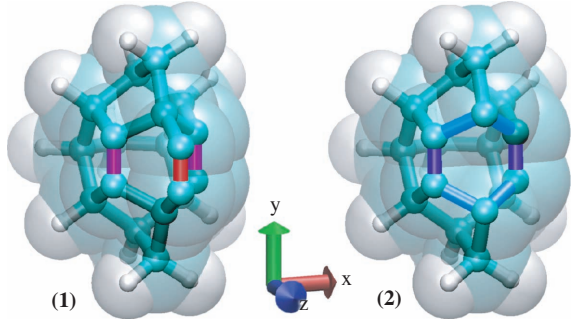

Fig. 1. DC10c, (left) with and (right) without, an attached carbon dimer. Colors in this illustration correspond to bond order: red for the dimer triple bond, purple for the adjacent double bonds, blue for the partial π-bonds in the unloaded tool, and green for σ-bonds.

Among the desirable properties of a mechanosynthetic tool are exoergic moiety transfer and favorable structural, electronic, and positional stability. The DC10c design for a carbon-transfer tool is the first reported to exhibit these desirable properties in combination. DFT calculations at the B3LYP/6-31G(d,p) level of theory have been used to characterize the energetics of key states and transformations of the tool-dimer complex (and several related structures). The results of these calculations include: strongly exoergic carbon dimer transfer from DC10c to structures with binding energies characteristic of graphene-, nanotube-, and diamond-like solids (for the model target structures described below, $\Delta E_{\text{transfer}} = -0.414$ to -0.261 aJ per atom), substantial barriers to structural rearrangement ($\geq$0.216 aJ) or fragmentation ($\sim$1.145 aJ) of the tool-dimer complex, and a large singlet–triplet energy gap ($\sim$0.240 aJ). The dimer is expected to have good positional stability as a consequence of its direct attachment to the stiff, polycyclic hydrocarbon structure of the tool, with calculated restoring-force gradients >150 Nm^{-1}. Further, the reactive dimer is well-exposed (Fig. 2), hence steric constraints in typical reactions are expected to be modest.

Simple, regular structures (e.g., lattices, sheets, and tubes) can serve as models for the energetic properties of more intricate structures. The difference between the binding energy of carbon atoms in a regular structure and in a loaded tool equals 1/2 the mean transfer energy, $\langle \Delta E_{\text{transfer}} \rangle$, for a sequence of operations that builds the structure from dimers placed by tools of that kind. If each operation places a dimer in a structurally identical site, then for each operation, $\Delta E_{\text{transfer}} = \langle \Delta E_{\text{transfer}} \rangle$ (this neglects edge sites in building solids and requires that a nanotube be chiral). If this binding energy is released during dimer transfer (rather than through a subsequent structural rearrangement), it provides the thermodynamic driving energy for the transfer. In the model target structures, the binding energy per atom ranges from 1.181 aJ in graphite to 1.105 aJ in (very narrow) carbon nanotubes 0.42 nm in diameter. (Sources: for graphite, Kittel;[22] for diamond, Schroeder;[23] and for nanotubes, Cabria et al.[24])

Transfer of a dimer from a saturated-hydrocarbon tool (e.g., Fig. 6, line **7** = H_4DC10c) presents energetic difficulties. The energy of the bound dimer is relatively high because the σ-bonds between the dimer and tool have angle strain and because the dimer itself contains two high-energy π-bonds. Although the transfer of a dimer to any of the target structures eliminates the angle strain and replaces one or more of the high-energy π-bonds with lower energy bonds, transfer from a saturated hydrocarbon tool also breaks two σ-bonds, leaving high-energy radicals on the tool. Calculations indicate that transfer of a dimer from H_4DC10c to model target structures is less favorable energetically than transfer from DC10c by about 0.278 aJ, and is endoergic in the nanotube case, where $\langle \Delta E_{\text{transfer}} \rangle = -0.136$ to $+0.017$ aJ.

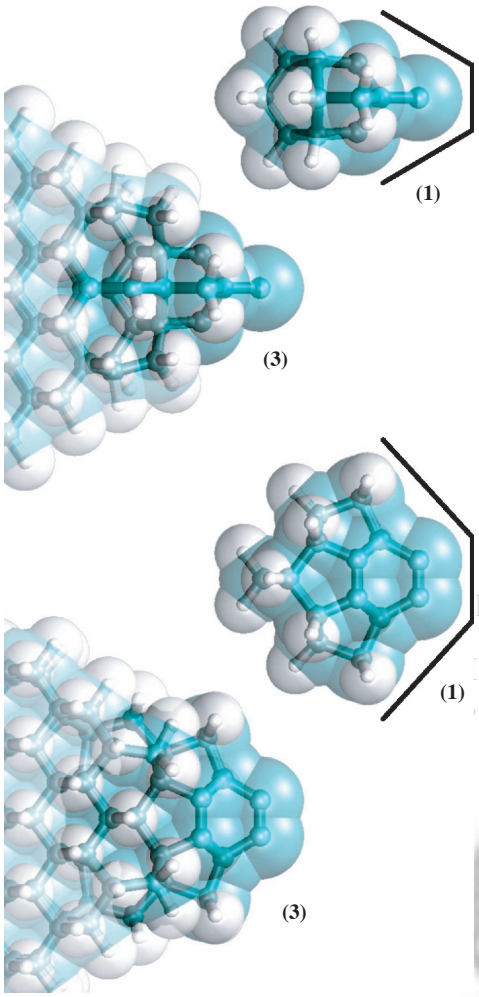

Fig. 2. Presented are (above) end and (below) side views of the DC10c tool, illustrating (to the right) the small structures used in the analysis of energetics and (to the left) one of many possible extended covalent structures in which the tool can be embedded. In use, these extended structures would interface to a mechanism that controls the relative positions of the tool and its target. Note that DC10c holds reactive dimers in a well-exposed position. Because the tool occupies a relatively small solid angle behind the dimer, this geometry limits potential interference between the tool and a target structure during dimer placement.

The DC10c design avoids this difficulty by avoiding the formation of radicals. It incorporates two π-bonds adjacent to the dimer binding site in such a way that the cleavage of the σ-bonds to the dimer creates a six-member π-bonded ring, electronically analogous to a strained benzene ring (Fig. 1). Calculations indicate strongly favorable transfer energies to the target structures, as noted above. Furthermore, the π-structure favors a concerted bond cleavage mechanism to regenerate the strained aromatic binding face of the empty tool, reducing the likelihood of states in which one end of a dimer remains bonded to the tool.

Section 3 of this article discusses the quantum chemistry of DC10c and related structures (including examining molecular geometries; binding energies of various structures; and energy differences between various structures, transition states, strained states, and multiplicities). Section 4 presents an operational analysis of the DC10c tool design, focusing on estimates of error rates resulting from various mechanisms.

3. COMPUTATIONAL METHODS

All structure optimizations (restricted and unrestricted wavefunctions) and normal mode calculations were performed with the 6-31G(d,p) Gaussian-type basis set[25] and B3LYP density functional.[26] The B3LYP density functional consists of the Becke 3-parameter hybrid exchange functional[27] (a linear combination of local density approximation, Becke gradient correction, and Kohn–Sham orbital-derived Hartree–Fock exchange energy) and the Lee–Yang–Parr nonlocal correlation functional.[28] The B3LYP density functional is a mainstay of current molecular DFT calculations for its accuracy both in structure and energies.[29] In light of the number and size of the many molecular structures considered in this study, DFT provides the clear balance/advantage of electron correlation (over Hartree–Fock theory) (HF) and reasonable computational costs (over post-HF methods such as Møller–Plesset Perturbation Theory or coupled-cluster methods). Normal mode analyses were performed for the calculation of zero-point energy (ZPE) corrections to specific ground-state energies for use in binding energy calculations. These ZPEs were scaled by 0.98 as discussed elsewhere.[29]

3.1. Small-Molecule Optimizations

Carbon dimer (C_2), ethyne ($HC{\equiv}CH$), ethene ($H_2C{=}CH_2$), and ethane ($H_3C{-}CH_3$) geometry optimizations were performed for the comparison of theory and experiment, subsequent comparison with their DC10c- and H_4DC10c-bound geometries, and component analyses of single and double bonds as they occur in the strained DC10c and H_4DC10c frameworks. Calculated carbon-bond lengths for these molecules are provided in Table I. Optimization of the minimum energy (singlet) C_2 dimer leads to a small overestimation (by 0.0013 nm) of its accepted bond length.[30] Similar results have been argued[31] as resulting from strong nondynamical correlation effects in C_2, but the general overestimation of carbon–carbon bond lengths calculated for small organic molecules with the B3LYP density functional contributes to some extent in this overall difference (a recent study of DFT structural comparisons of small hydrocarbons can be found in Neugebauer and Häfelinger[32]). Efforts to improve theoretical agreement are not undertaken here for C_2 because (1) the computational expense required for calculating all other structures at the same level of theory is substantially beyond feasibility and (2) the C_2 dimer does not, by itself, occur in any of the presented structures (the introduction of any external σ-bonding source to C_2 results in the dimer adopting typical alkyne carbon-carbon bond lengths). Bond length

RESEARCH ARTICLE

Table I. B3LYP/6-31G(d,p) and experimental carbon–carbon bond lengths, in nanometers. Experimental values are taken from Huber and Herzberg[30] (for C_2 dimer) and Neugebauer and Häfelinger[32] (for the others).

	C_2	HC≡CH	$H_2C{=}CH_2$	$H_3C{-}CH_3$
Experiment	0.1243	0.1203	0.1331	0.1528
RB3LYP singlet	0.1256	0.1206	0.1331	0.1530
UB3LYP triplet	0.1203	0.1342	0.1543	0.1489

agreement between theory and experiment is otherwise excellent in the series. The triplet states of these molecules were also optimized for later comparison. Bond length reduction in triplet $H_3C{-}CH_3$ results from the loss of a single hydrogen atom and subsequent rehybridization of the CH_2 carbon to sp^2.

3.2. Empty DC10c and H_4DC10c Structures

Pertinent structural information for singlet and triplet geometries is provided in Table II (with key in Fig. 3) for DC10c (in which the framework includes π-bonding) and for a variant structure, H_4DC10c, (in which the framework has only σ-bonding), in their "empty" states (without a bound dimer). The singlet and triplet forms of both empty structures optimize to C_{2v}-symmetry minima. Despite significant structural deformation in the benzene-like π-conjugation pathway, the empty DC10c tool optimizes to a ground-state singlet with a significant decrease in single/double bond length alternation relative to the optimized triplet form. The ground-state singlet DC10c tool's energy lies 0.187 aJ below its singlet-geometry triplet energy and 0.075 aJ below its geometry-optimized triplet. In contrast, the empty H_4DC10c structure optimizes to a ground-state triplet that lies 0.174 aJ below its geometry-optimized singlet, consistent with the localization of unpaired electrons to the framework-separated dimer-binding [C_B, $C_{B'}$] positions.

The drive towards π-conjugation in the binding face of the empty DC10c tool is apparent from bond length comparisons of the optimized singlet (0.1386 vs. 0.1427 nm) and triplet (0.1342 vs. 0.1508 nm) (Table II and Fig. 3). The structural changes in the triplet DC10c empty tool are

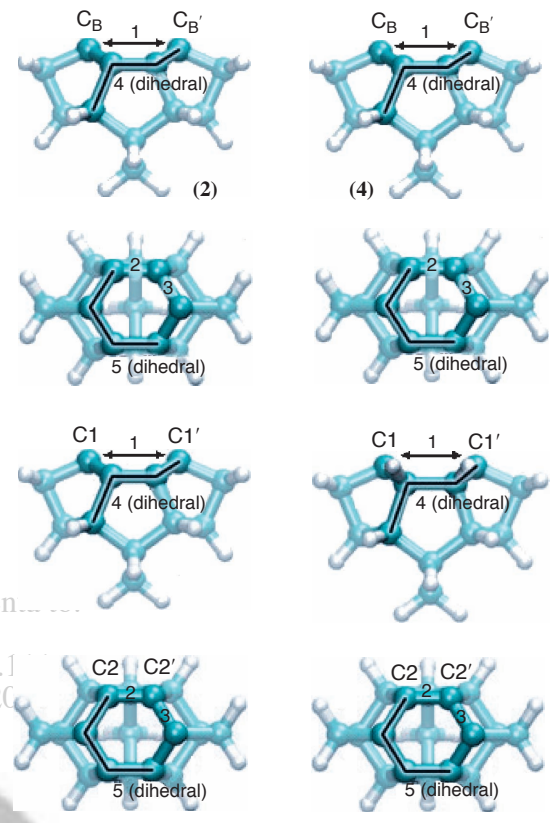

Fig. 3. Empty DC10c and H_4DC10c structures (see Table II for the values of the labeled dimensions).

similar to those of the triplet H_4DC10c structure, where the dimer-binding orbitals of the [C_B, $C_{B'}$] atoms are effectively decoupled from one another and the remainder of the framework. The decoupling of the [C_B, $C_{B'}$] carbons in the DC10c triplet optimization leads to single/double bond lengths consistent with the small molecule results (Table II). Despite an increase in single/double bond length alternation in the empty DC10c tool, the [C_B, $C_{B'}$] separation changes very little between the optimized singlet and triplet forms. This structural commonality will be of interest in the analysis of dimer binding. The direction of the π-conjugation changes in the strained binding face of DC10c mirror those changes calculated for benzene, where

Table II. B3LYP/6-31G(d,p) bond lengths (in nanometers), dihedral angles (in degrees), and singlet-triplet energy differences (in attojoules) for the empty DC10c and H_4DC10c structures. See Figure 3 for the labeling scheme.

	Multiplicity	1: Bond length (nm)	2: Bond length (nm)	3: Bond length (nm)	$4_{Dihedral}$ (°)	$5_{Dihedral}$ (°)	$E_{Relative}$ (aJ)
DC10c	Singlet	0.2823	0.1386	0.1427	118.3	38.7	0.000
	Triplet	0.2847	0.1342	0.1508	123.6	46.9	0.075
H_4DC10c	Singlet	0.2764	0.1515	0.1505	111.5	43.8	0.174
	Triplet	0.2891	0.1540	0.1518	111.9	41.9	0.000

	Multiplicity	"Short" (nm)	"Long" (nm)	$Diameter_{C-C}$ (nm)
Benzene	Singlet	0.1397	0.1397	0.2793
	Triplet	0.1347	0.1476	0.2847

triplet-state geometry optimization results in unpaired spin separation to *para*-positions and a reduction of the joining double-bond lengths to values approaching those for ethene (0.1331 nm).

3.3. Loaded DC10c and H_4DC10c Structures

Diagnostic structural features of the "loaded" (containing a bound molecule) DC10c and H_4DC10c structures are labeled in Figure 4 and listed in Table III. All loaded structures optimize to ground-state singlets of C_{2v} symmetry. The binding energies (empty + dimer/moiety → loaded) for DC10c (empty ground-state singlet) and H_4DC10c (empty ground-state triplet) are also provided in Table III. The formation of two σ-bonds to structures with HC≡CH and $H_2C{=}CH_2$ comes at the expense of a broken π-bond in each case, reducing the binding energies of these molecules relative to that the C_2 dimer, which binds by two external σ-bonds with no formal change in its π-bonding. The predicted DC10c binding energies decrease (relative to H_4DC10c) by 8.1% (C_2) to 7.4% (C_2H_2). The binding faces of DC10c and H_4DC10c are remarkably similar when both structures are compared with identical bound molecules. The differentiation between single- and double-bonds in the loaded DC10c tool is enhanced relative to both the DC10c empty singlet and triplet states. The absence of benzene-like π-delocalization and increased single/double bond length alternation in the moiety-binding DC10c tool is reminiscent of the direction of structural changes in the empty triplet DC10c tool. The three most important structural features shared by DC10c and H_4DC10c (with the same bound molecule) are (1) the dimer-binding σ-bond lengths (labeled [2] in Table III), (2) the carbon–carbon bond lengths in the bound moieties (labeled [4] in Table III), and (3) the [C_B, $C_{B'}$] distances (labeled [5] in Table III). The [C_B, $C_{B'}$] distance is, perhaps, the most important structural link between DC10c and H_4DC10c, a fortuitous result of angle and bond strain in the two structures that make the empty environments different but the loaded structures very similar. This nearly identical [C_B, $C_{B'}$] separations result in (structurally) nearly identical

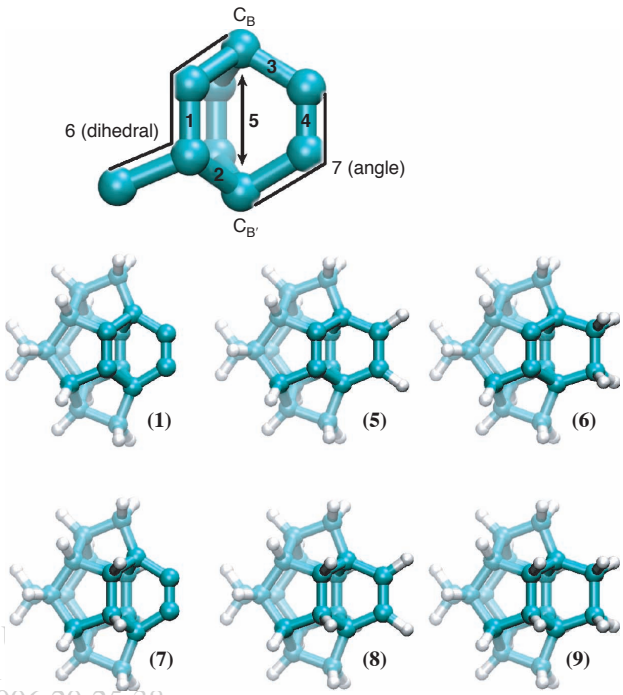

Fig. 4. DC10c and H_4DC10c structures with bound moieties. (See Table III for the values of the labeled dimensions.)

binding environments, thereby leading to similar bound molecule geometries. The [C_B]-to-bound-molecule bond lengths, at 0.1498 to 0.1544 nm, are all well within the σ-bonding regime. The bound C_2 dimer changes from its isolated structure to that of a strained alkyne (labeled as [—C≡C—] when referred to in its bound form), undergoing a decrease in C≡C bond length. The HC≡CH molecule binds to form a slightly strained alkene (bound form: [—HC=CH—]). The $H_2C{=}CH_2$ molecule binds as a strained alkane (bound form: [$—H_2C—CH_2—$]) in an eclipsed conformation. Carbon–carbon bond length elongation in this entire series is a result of the non-optimal [C_B, $C_{B'}$] separation from what the bound moieties would prefer in unstrained molecules. The optimization of the $H_2C{=}CH_2$-bound structures to C_{2v} symmetry minima—not to slightly staggered conformations to relieve repulsive H—H interactions—indicates the extent of this carbon–carbon bond stretching and the rigidity of the binding face.

Table III. B3LYP/6-31G(d,p) bond lengths (in nanometers), bond angles (in degrees of arc), and moiety binding energies (in attojoules) for the DC10c and H_4DC10c structures. See Figure 4 for the labeling scheme.

		Dimension					$6_{Dihedral}$	7_{Angle}	$E_{binding}$	$ZPE^a_{binding}$
	Bound fragment	1 (nm)	2 (nm)	3 (nm)	4 (nm)	5 (nm)	(°)	(°)	(aJ)	(aJ)
DC10c	[—C≡C—]	0.1323	0.1571	0.1498	0.1238	0.2681	128.3	118.8	1.175	1.145
	[—HC=CH—]	0.1321	0.1548	0.1525	0.1354	0.2605	129.0	114.2	0.722	0.682
	[$—H_2C—CH_2—$]	0.1326	0.1539	0.1544	0.1603	0.2626	128.6	109.4	0.645	0.605
H_4DC10c	[—C≡C—]	0.1513	0.1578	0.1508	0.1243	0.2665	115.6	118.1	1.279	1.242
	[—HC=CH—]	0.1510	0.1564	0.1524	0.1359	0.2591	116.3	113.8	0.779	0.734
	[$—H_2C—CH_2—$]	0.1516	0.1551	0.1543	0.1614	0.2617	116.3	109.0	0.699	0.654

[a] $ZPE_{binding}$ energies are ZPE-corrected.

DC10c binding a C_2 dimer is the most important structure in this study and warrants extra attention. The C_2 dimer is bound to the open face of the empty DC10c tool by two strained σ-bonds. With the removal of binding-face π-delocalization upon inclusion of the C_2 dimer, the loaded DC10c tool combines two different, strained structural motifs familiar in organic chemistry. The strained double-bonds flanking the bound C_2 dimer are examples of pyramidal alkenes, whose stabilities and reactivities have been extensively studied.[33] Binding strain in the σ-bonding to the C_2 dimer results in the tool-dimer interaction adopting a geometry similar to that calculated for the strained cyclic hydrocarbon *ortho*-cyclohexyne.[34] The cyclohexyne [—C≡C—] linkage is under reduced strain relative to DC10c, as noted by the increased separation of the adjoining ring carbons (0.3189 nm), the decreased C≡C bond length in the B3LYP/6-31G(d,p) structure (0.1221 nm), and the increased angle between each adjoined ring carbon and dimer (131.6°). The energy differences of the ground-state singlet and geometry-optimized triplet cyclohexyne, DC10c, and H_4DC10c structures are also useful for highlighting the strain on the alkyne (these comparisons are possible in all three structures because triplet-state optimization leads to structural changes almost entirely localized to the triple bonds). Optimization of the cyclohexyne triplet geometry yields a ring similar in structure to that of cyclohexene, including a C≡C bond length of 0.1336 nm and a ring-dimer angle of 125.0°. The optimized singlet–triplet energy difference here is 0.281 aJ. The optimizations of the triplet states for the C_2-bound DC10c and H_4DC10c structures result in similar geometric changes to the C_2 dimers and reduced singlet–triplet energies (DC10c = 0.240 aJ, H_4DC10c = 0.223 aJ).

3.4. Singlet–Triplet Transitions

The consideration of the DC10c and H_4DC10c triplet states is important in the analysis of loaded structure stability (specifically for the C_2 dimer-bound states). The energies and optimized geometries of the triplet states also serve as useful probes of binding strain in these structures. Three bond lengths that serve as diagnostic measures of the direction of structural changes in the optimized triplet geometries are provided in Table IV and identified in Figure 4. Triplet-state H_4DC10c optimizations indicate that the framework is quite inflexible, with all crucial structural changes from the imposition of two unpaired electrons occurring in the C_2 dimer. In the case of [—H_2C—CH_2—], triplet-state optimization leads to a breaking of the stretched C—C σ-bond (the triplet equilibrium C—C distance is 0.330 nm; the triplet energy of the ground state singlet geometry lies 1.197 aJ above the singlet energy). This σ-bond fragmentation results in a 0.033 nm increase of the $[C_B–C_{B'}]$ distance and a smaller (0.004 nm) increase of the more constrained $[C_B–C_{B'}]$ distances. The [—C≡C—] and [—HC=CH—] H_4DC10c structures deform in their triplet optimizations at the π-bonds nearly identically to the free ligands, with slight elongation of the bond lengths due to $[C_B–C_{B'}]$ strain.

The presence of strained framework double bonds in the binding face of DC10c has the effect of introducing framework structural changes upon triplet optimization of the [—HC=CH—] and [—H_2C—CH_2—] structures. In these two structures, triplet optimization leads to an approximately 0.008 nm elongation of the binding face along the $[C_B–C_{B'}]$ axis (both double bonds and, consequently, the $[C_B–C_{B'}]$ distance). The [—HC=CH—] and [—H_2C—CH_2—] carbon distances are affected negligibly. The angle strain in the C_2 dimer found previously to reduce the singlet–triplet energy gap between the cyclohexyne and loaded structures makes the C_2 dimer, and not the strained double bonds, the primary location of structural change upon DC10c triplet optimization. Localization of structural changes to the C_2 dimer of both the [—C≡C—] DC10c and H_4DC10c structures leads to these two forms having the most similar singlet–triplet energy gaps of the structure series (Table IV).

3.5. Tool Failure Modes and Dimer Displacements

Large dimer displacements can cause reaction failures in mechanosynthesis, as can rearrangement of the tool framework. Figure 5 illustrates the geometry of selected alternative minima of the loaded DC10c tool (state (**1**)). Calculation of the energetic accessibility of these structures is necessary for the analysis of failure states of the

Table IV. B3LYP/6-31G(d,p) bond lengths/atom distances (in nanometers) and singlet–triplet energy differences (in attojoules) for the DC10c and H_4DC10c structures. See Figure 4 for the labeling scheme.

		DC10c		H_4DC10c	
Dimension	Bound fragment	Singlet	Triplet	Singlet	Triplet
1	[—C≡C—]	0.1323	0.1329	0.1513	0.1513
	[—HC≡CH—]	0.1321	0.1401	0.1510	0.1518
	[—H_2C—CH_2—]	0.1326	0.1406	0.1516	0.1551
4	[—C≡C—]	0.1238	0.1368	0.1243	0.1360
	[—HC≡CH—]	0.1354	0.1359	0.1359	0.1592
	[—H_2C—CH_2—]	0.1603	0.1617	0.1613	3.303
5	[—C≡C—]	0.2681	0.2648	0.2665	0.2611
	[—HC=CH—]	0.2605	0.2688	0.2591	0.2648
	[—H_2C—CH_2—]	0.2626	0.2720	0.2617	0.2948

		Triplet energies[a]		Triplet energies[a]	
	Bound fragment	$1 \rightarrow 3$	$1 \rightarrow 3$(E)	$1 \rightarrow 3$	$1 \rightarrow 3$(E)
	[—C≡C—]	0.240	0.283	0.223	0.307
	[—HC≡CH—]	0.232	0.311	0.502	0.646
	[—H_2C—CH_2—]	0.222	0.304	0.467	1.197

[a] $1 \rightarrow 3$ = (geometry-optimized singlet) → (geometry-optimized triplet); $1 \rightarrow 3$(E) = (geometry-optimized singlet) → (singlet-geometry triplet).

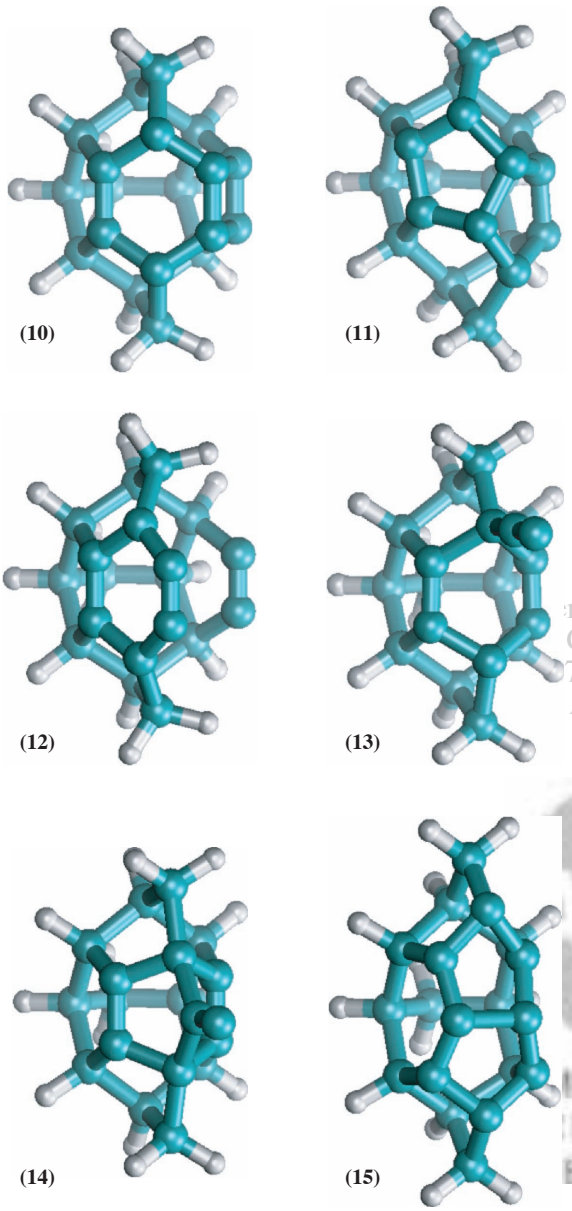

Fig. 5. Configurations examined as possible tool failure modes (see Fig. 6 for a graphical summary of the relative energies of these structures and of selected transition states).

loaded tool; calculation of the energy of lower-amplitude displacements of the dimer is necessary to estimate the rate of failure during dimer placement operations. As indicated in Section 4.4, displacement coordinates with mechanical stiffness $\geq$150 Nm^{-1} are compatible with highly reliable placement operations at 300 K.

Together, the two atoms of a dimer have six degrees of freedom; these can be decomposed into three bond-stretching coordinates and three bond angle-bending coordinates. Of the three bond-stretching coordinates, one (stretching of the dimer triple bond) is extremely stiff, moving toward a cleaved state that is both energetically inaccessible and subject to immediate recombination. The remaining two bond-stretching coordinates can be decomposed into stretching of one bond, moving toward state (**13**) (see Fig. 5), and stretching of both bonds, moving toward dimer cleavage. These bond-stretching coordinates are expected to be stiff (well over 200 Nm^{-1}). State (**13**) is calculated to be above state (**1**) by 0.304 aJ, and dimer cleavage from DC10c is calculated to require 1.145 aJ.

The bond angle-bending coordinates allow larger thermal displacements of the dimer. These can be decomposed into rotation about the z-axis (coupled with motion towards $-z$), rotation about the x-axis (coupled with motion in both y and z), and displacement along the x-axis (coupled with motion towards $-z$). The calculated force gradients resisting these bending displacements are all >150 Nm^{-1}.

Rotation about the x-axis moves toward state (**14**), which is above (**1**) by 0.304 aJ and is not a local minimum of the potential energy. Displacement along the x-axis moves toward state (**10**), which is *below* (**1**) (at −0.165 aJ), but is rendered relatively inaccessible by a barrier calculated[35] to be >0.4 aJ. A 90° rotation around the z-axis moves the dimer to a position above (**15**), but that state is above state (**1**) by 0.372 aJ. A relatively accessible transition leads to state (**11**), which is somewhat *below* state (**1**) (at −0.099 aJ) and separated from it by a barrier calculated to be 0.216 aJ. In another transition, cleavage of two framework bonds leads to state (**12**) through an electronic reorganization consistent with a retro-Diels–Alder reaction. State (**12**) is only 0.101 aJ above state (**1**), and the (**1**) → (**12**) transition barrier is the lowest identified, calculated to be 0.213 aJ. Occurrence of the transition (**1**) → (**12**) thus appears to be the chief constraint determining the temperature/reliability trade-off relationship for the DC10c tool. Figure 6 diagrams the relative energies of these and several other states of interest.

4. OPERATIONAL RELIABILITY

Assuming good environmental control (i.e., very rare encounters with stray molecules[8]), failures will result either from unwanted transitions in the tool structure (*tool failure*) or from unintended outcomes of attempted reactive encounters (*reaction failure*). Tool failures will cause subsequent reaction failures, but are usefully distinguished because they can occur at any time before the reactive encounter.

A transfer operation might fail because of structural damage to the tool before a transfer attempt, because of incorrect placement, electronic excitation, or failure to attach the dimer during an attempt, or because the tool fails to release the dimer afterward, when the tool is retracted. The frequency of these failure modes can be estimated through calculations of the relative energies of selected structures and states, and through estimates of the frequency of damage caused by external radiation sources. Much of the following discussion is generic with respect to mechanosynthetic tools and operations, rather than specific to DC10c and dimer transfer.

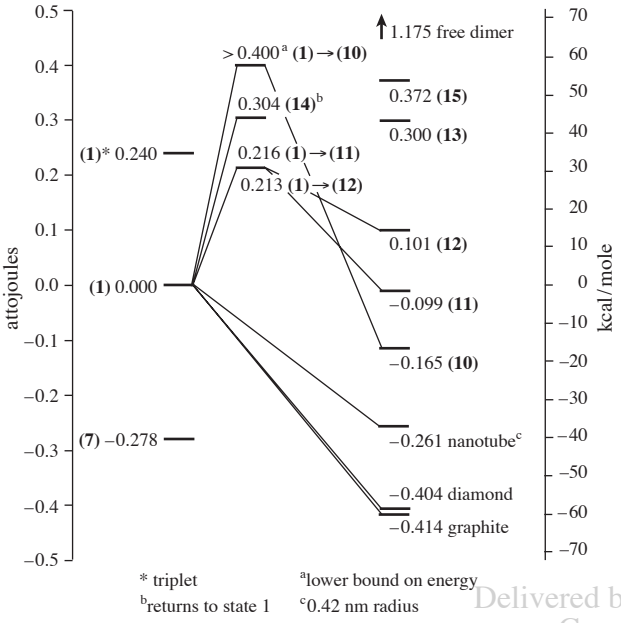

Fig. 6. Energy changes associated with dimer transfers from the loaded DC10c tool (line **1**) to graphite, diamond, a 0.42 nm nanotube, H_4DC10c (line **7**), and free space. Also diagrammed are the energies of electronic excitation of (**1**), and of selected structural rearrangements and transition states. Corresponding structure numbers are provided in parentheses.

4.1. Reaction Failure Caused by Non-Transfer

Tool retraction must not remove the moiety to be transferred, else a non-transfer failure occurs. The most straightforward model for the transfer process treats the encounter of a tool and target as equilibrating the probabilities (equivalent to mean concentrations) of the moiety remaining in the target-side potential well vs. exiting in the tool-side potential well (i.e., a non-transfer failure). At a temperature T, the probability of non-transfer can be estimated as

$$P_{\text{fail}}(T) = \left[1 + \exp\left(\frac{\Delta E_{\text{transfer}}}{k_B T}\right)\right]^{-1}$$

where $P_{\text{fail}}(T)$ is the probability that retraction removes the moiety together with the tool. This model would, however, be inapplicable if complex or asymmetric potentials were to leave the dimer in a metastable well after the encounter. Circumstances causing this phenomenon (with favorable effects) have been noted by Merkle.[36] An accurate treatment of non-transfer errors would require a study of the time-dependent potential energy surface governing dimer motion during an encounter, which is beyond the scope of this paper.

For transfer of a dimer to diamond, the calculated transfer energy is −0.404 aJ and the equilibrium model predicts $P_{\text{fail}}(300) < 10^{-42}$, with a lower error probability for transfer that extends a graphite sheet ($\sim 10^{-45}$) and a higher error probability ($\sim 10^{-36}$) for transfer to a 0.42 nm carbon nanotube. For transfer of a dimer to a model diradical site on an irregular hydrocarbon structure (H_4DC10c again), the calculated $\Delta E_{\text{transfer}} = -0.278$ aJ and the equilibrium model predicts $P_{\text{fail}}(300) \approx 10^{-29}$. Thus, for a range of model structures, non-transfer errors will be quite rare at ambient temperatures.

4.2. Reaction Failure Caused by Activation Barriers

Attachment of a moiety to a target will, for some targets, proceed without an activation barrier. Applied mechanical force can, for some additional targets, reshape the reaction potential energy surface to eliminate barriers found in the force-free case. Data from a DFT study of related tools[21] indicates barriers of less than 0.02 aJ for dimer transfer to a bare diamond (100) surface. Barriers of this form and magnitude would be reduced to zero by a modest force, on the order of 20 pN ($\sim$0.01 times the mechanical strength of a typical covalent bond). In reactions where the net barrier (including any applied force) is zero, the reliability of reactions will increase with decreasing temperature, leading to a monotonic temperature/reliability trade-off curve.

Where a barrier exists, thermal activation will result in barrier crossing at a rate that can be estimated as

$$k_{\text{transfer}}(T) = A \exp\left(\frac{-\Delta E_{\text{a, transfer}}}{k_B T}\right)$$

This standard for reaction kinetics model has an Arrhenius dependence upon temperature and free energy. The pre-exponential factor A will be approximated here as 10^{13} s^{-1} (on the order of a molecular vibrational frequency). For a process with a tool dwell-time τ, the failure probability is

$$P_{\text{notransfer}} = \exp(-k_{\text{transfer}}\tau)$$

With $\tau = 1$ ns and $\Delta E_{\text{a, transfer}} = 0.02$ aJ, $P_{\text{notransfer}} \approx 10^{-35}$ at 300 K.

Note that the energy required for tool retraction (which completes the transfer operation) is to be provided by an external mechanical source and accordingly does not enter into this failure analysis.

4.3. Reaction Failure Caused by Electronic Excitation

Triplet and singlet states differ in reactivity, and triplet states may have a long lifetime relative to the duration of a transfer operation. Accordingly, a conservative treatment of reliability must assume that using a ground-state singlet tool in a triplet state will cause reaction failure. This occurs with a probability per operation

$$P_{\text{fail}}(T) = \left[1 + \exp\left(\frac{\Delta E_{\text{triplet}}}{k_B T}\right)\right]^{-1}$$

For DC10c, the dimer-tool complex is predicted to be a ground-state singlet with $\Delta E_{\text{triplet}} = 0.240$ aJ, hence $P_{\text{fail}}(300) \approx 10^{-25}$.

4.4. Reaction Failure Caused by Mechanical Displacement

Displacement of a tool from its intended target can cause failure by enabling an unwanted reaction to occur. Offsets are of two fundamentally different sorts: *thermal* displacement caused by fluctuations about the equilibrium tool position, and *static* displacement of the equilibrium position itself, caused by a displacement in the positioning mechanism (for example, caused by thermal gradients and device hysteresis). Design and analysis indicate that in the intended system context static displacement can be restricted to $\ll 0.01$ nm, a negligible fraction of the distance between competing reactive sites.[8] Unavoidable thermal displacements, in contrast, can be relatively large.

Configurations with unacceptable displacements $\Delta x_{\mathrm{fail},\,i}$ have stored elastic energy

$$\Delta E_{i,\,\mathrm{elastic}} = \frac{1}{2} k_{\mathrm{s,\,i}} \Delta x_{\mathrm{fail},\,i}^2$$

leading to an approximate failure probability

$$P_{i,\,\mathrm{fail}}(T) \approx \exp\left(\frac{-\Delta E_{i,\,\mathrm{elastic}}}{k_{\mathrm{B}} T}\right)$$

The actual relationship between reliability and stiffness will depend on details of the tool-target interaction potential; this approximation will be most accurate when alternative sites are similar in both reactivity and distance (measured along the tool-approach coordinate). A loaded DC10c tool holds a carbon dimer with a stiffness $\sim$150 Nm^{-1} in its softest bending mode (perpendicular to the dimer axis), but compliance (reciprocal stiffness) elsewhere in the system will reduce the overall stiffness of tool positioning. A system-level design analysis[8] indicates that a reasonable value for overall stiffness is $k_{8,\,i} \approx 20$ Nm^{-1} (for all axes i) leading to $P_{i,\,\mathrm{fail}}(300) \approx 10^{-24}$ if $\Delta x_{\mathrm{fail},\,i}$ is 0.15 nm (a typical bond length).

4.5. Tool Failure Caused by Thermal Structural Rearrangement or Cleavage

Unimolecular rearrangement or cleavage of a tool structure (loaded or unloaded) will typically cause a subsequent reaction failure. For good reliability, the barriers to thermally activated rearrangement or cleavage must be $\gg k_{\mathrm{B}} T$. An estimate of the frequency of tool failure *via* a mode i with barrier $\Delta E_{\mathrm{a},\,i}$ is roughly

$$k_{\mathrm{fail},\,i}(T) = A \exp\left(\frac{-\Delta E_{\mathrm{a},\,i}}{k_{\mathrm{B}} T}\right)$$

In this expression, the activation energy $\Delta E_{\mathrm{a},\,i}$ is a difference of ZPE-corrected Helmholtz free energies, but the entropic component of $\Delta E_{\mathrm{a},\,i}$ will be small for structural rearrangement or cleavage because all coordinates in both states (except for the reaction coordinate in the transition state) have only vibrational degrees of freedom, and of similar magnitudes. The added translational degree of freedom in the transition state reduces its zero-point energy by $\sim$0.008 aJ, which is negligible in comparison to the energy barriers considered here.

As described in Section 3.5, the lowest value of $\Delta E_{\mathrm{a},\,i}$ is found in the rearrangement (**1**) $\rightarrow$ (**12**), $\sim$0.213 aJ. The corresponding value of $k_{\mathrm{fail},\,i}(300)$ is $\sim 10^{-10}$ s^{-1} (corresponding to a lifetime of many years). Other rearrangements appear to have substantially larger values of $\Delta E_{\mathrm{a},\,i}$ indicating that they make a negligible contribution to the overall failure rate.

4.6. Tool Failure Caused by Radiation Damage

Non-thermal electromagnetic radiation with energies up to the ultraviolet can readily be excluded by metallic barriers less than a micron thick,[8] but higher-energy radiation (both electromagnetic and particulate) causes structural damage and cannot be fully excluded. Terrestrial background radiation (which rarely exceeds 0.5 rad yr^{-1}) causes damaging events at a rate on the rough order of $\sim 10^{7}$ kg^{-1} s^{-1}. Failure rates associated with damage to the tool structure considered here accordingly will be on the rough order of 10^{-32}. The failure rate of radiation-sensitive mechanisms associated with a tool-using subsystem in a mechanosynthetic device will be orders of magnitude larger, owing to their larger size; a reasonable estimate[8] is on the rough order of 10^{-19} s^{-1}.

4.7. Failure Summary

The tool-failure mechanisms examined above cause failures at rates described in units of failures per second. The radiation damage rate is approximately temperature-independent; the rearrangement rates are steeply temperature-dependent. Which mode dominates therefore depends on temperature: at 300 K, rearrangement is calculated to occur at a rate of $\sim 10^{-10}$ s^{-1}, orders of magnitude greater than the 10^{-19} s^{-1} failure rate estimated for radiation damage. At $\sim$200 K, the rates cross; at 70 K the rearrangement rate falls to $\sim 10^{-83}$ s^{-1}.

Reaction-failure mechanisms, in contrast, have rates described in units of failures per operation. Reaction failures place the target and tool in unintended states, but do not necessarily damage the tool. The largest reaction-failure rates in the sample calculations are on the order of 10^{-24} per operation; this is compatible with the fabrication of gram-scale structures without misplaced atoms. In practice, accomplishing this would require both reduced temperatures ($\sim$200 K) to increase tool lifetime and the use of fabrication processes that exploit enormous parallelism. Further, the defect rate of a completed product structure would be elevated above this extremely low level by radiation damage accumulated during its fabrication.

5. CONCLUSIONS

A B3LYP/6-31G(d,p) study indicates that the DC10c tool can transfer carbon dimers to structures with binding energies in the range of graphite, diamond, and narrow nanotubes. When combined with a hydrogen-transfer tool (or perhaps when used to transfer hydrogen-containing moieties; e.g., ethyne from (**5**) or ethene from (**6**)), DC10c should enable the synthesis of a wide range of hydrocarbon structures. Since mechanosynthetic placement of dimers permits stepwise control of molecular assembly, this range of structures can include intricate members of a large combinatorial class. Much as an ink-jet printhead can be used to create intricate two-dimensional patterns by placing droplets under programmed positional control, so a DC10c placement tool could be used to create intricate three-dimensional structures by placing carbon dimers under programmed positional control (a fundamental difference, however, is that dimer placement cannot be arbitrary, but must be directed to suitable reactive sites). Some stable structures will presumably be inaccessible through this technique, yet the accessible set will apparently be enormous, including a wide range of atomically precise mechanical and electronic devices. Calculations indicate that (with mild constraints on the geometry and reactivity of the target sites) a mechanosynthetic system using DC10c tools could (at temperatures ~200 K) build structures with a stepwise error rate on the order of 10^{-24}. In diffusion-based organic synthesis, in contrast, error rates on the order of 10^{-2} (yields of 99%) are considered quite favorable. Accordingly, the scale and complexity of error-free structures that can be made by advanced mechanosynthetic systems exceeds that of conventional synthesis by a factor on the rough order of 10^{22} (provided the product structure has good stability, and neglecting the accumulation of radiation damage during its fabrication).

The favorable shape and reaction energetics of DC10c appear inconsistent with the speculation[37] that fundamental physical principles will prevent mechanosynthetic tools from transferring reactive moieties to target sites, either because of prohibitively strong binding ("sticky fingers") or prohibitively large steric bulk ("fat fingers").

Much remains to be done to explore tools, reaction processes, and potential applications for advanced mechanosynthetic systems. Natural directions for further theoretical research include the search for structures with a improved temperature/reliability trade-offs, studies of processes for tool preparation,[13, 38] exploration of reaction potentials for the transfer of moieties to various targets, the design of transfer tools for a wider range of moieties (for example, containing elements other than hydrogen and carbon), and the design both of useful structures and of mechanosynthetic processes for making them. Perhaps of greatest importance is the implementation of a technology base that is in turn able to implement machine-phase mechanosynthetic systems. This long-term objective, together with exploitation of opportunities resulting from intermediate advances, suggests a productive direction for intertwined theoretical and laboratory development.[39]

Acknowledgments: We would like to thank Nanorex and the Foresight Institute for providing machine resources in support of this study. Graphics were generated with VMD.[40]

References

1. R. Warmuth, *J. Inclusion Phenom. Macrocyclic Chem.* 37, 1 (**2000**).
2. H. J. Lee and W. Ho, *Science* 286, 1719 (**1999**).
3. D. Huang, H. Uchida, and M. Aono, *J. Vac. Sci. Technol. B* 12, 4 2429 (**1994**).
4. N. Oyabu, Ó. Custance, I. Yi, Y. Sugawara, and S. Morita, *Phys. Rev. Lett.* 90, 176102 (**2003**).
5. S. W. Hla, L. Bartels, G. Meyer, and K. H. Rieder, *Phys. Rev. Lett.* 85, 2777 (**2000**).
6. K. E. Drexler and J. S. Foster, *Nature* 343, 600 (**1990**).
7. K. E. Drexler, *J. Vac. Sci. Technol. B* 9, 1394 (**1991**).
8. K. E. Drexler, *Nanosystems: Molecular Machinery, Manufacturing, and Computation*, John Wiley & Sons, New York (**1992**).
9. K. E. Drexler, *Ann. Rev. Biophys. Biomol. Structure* 23, 337 (**1994**).
10. R. C. Merkle, *Nanotechnology* 7, 210 (**1996**).
11. R. C. Merkle, *Nanotechnology* 8, 23 (**1997**).
12. R. C. Merkle, *Nanotechnology* 10, 315 (**1999**).
13. R. C. Merkle, *Nanotechnology* 8, 149 (**1997**).
14. C. Phoenix, *J. Evol. Tech.* 13 (**2003**). Available at http:// jetpress.org/volume13/Nanofactory.htm
15. K. E. Drexler, *Proc. Nat. Acad. Sci.* (*USA*) 78, 5275 (**1981**).
16. R. C. Merkle, *Trends Biotech.* 17, 271 (**1999**).
17. R. C. Merkle, *Nanotechnology* 11, 89 (**2000**).
18. S. P. Walch and R. C. Merkle, *Nanotechnology* 9, 285 (**1998**).
19. C. B. Musgrave, J. K. Perry, R. C. Merkle, and W. A. Goddard III, *Nanotechnology* 2, 187 (**1991**).
20. R. C. Merkle and R. A. Freitas, Jr., *J. Nanosci. Nanotechnol.* 3, 319 (**2003**).
21. D. J. Mann, J. Peng, R. A. Freitas, Jr., and R. C. Merkle, *J. Comput. Theor. Nanosci.* 1, 71 (**2004**).
22. C. Kittel, *Introduction to Solid State Physics,* 6th ed., John Wiley & Sons (**1986**).
23. D. V. Schroeder, *An Introduction to Thermal Physics,* Addison–Wesley (**2000**).
24. I. Cabria, J. W. Mintmire, and C. T. White, *Phys. Rev. B* 67, R121406 (**2003**).
25. O. C. Hariharan and J. A. Pople, *Theoret. Chim. Acta* 28, 213 (**1973**).
26. Density functional theory (DFT) calculations were performed with the PC-GAMESS version[41] of the GAMESS-US quantum chemistry package.[42]
27. A. D. Becke, *J. Chem. Phys.* 98, 5648 (**1993**).
28. C. Lee, W. Yang, and R. G. Parr, *Phys. Rev. B* 37, 785 (**1988**).
29. J. B. Foresman and A. E. Frisch, *Exploring Chemistry with Electronic Structure Methods,* Gaussian, Inc., Pittsburgh, PA (**1996**).
30. K. P. Huber, G. Herzberg, *Constants of Diatomic Molecules,* Van Nostrand Reinhold (**1979**).
31. J. M. L. Martin, J. El-Yazal, and J. P. François, *Chem. Phys. Lett.* 242, 570 (**1995**).
32. A. Neugebauer and G. Häfelinger, *J. Molec. Struct. Thermochem.* 578, 229 (**2002**).

33. The theory and chemistry of the pyramidal alkenes has been considered in detail in W. T. Borden, *Chem. Rev.* 8, 1095 **(1989)**. Of particular comparative interest is tricyclo-[3.3.2.0^{3,7}]dec-3(7)-ene, a molecule with a somewhat reduced calculated alkene pyramidalization relative to the calculated DC10c structure (approximately 45.7°) that has undergone spectroscopic characterization by matrix isolation [T. K. Yin, F. Miyake, G. E. Renzoni, W. T. Borden, J. G. Radziszewski, and J. Michl, *J. Am. Chem. Soc.* 108, 3544 **(1986)**]. The demonstration of reactive-molecule persistence for spectroscopic characterization in matrix isolation studies is consistent with the general scope of machine-phase mechanosynthesis, where reactivity between moieties occurs only with the availability of other reactants (or workspaces) and unwanted side-reactivity between components can be removed by design.

34. *Ortho*-cyclohexyne and *ortho*-cycloheptyne cannot be isolated as single molecules due to their high reactivity. While the isolated molecule is highly reactive (as expected from significant angle strain and as utilized in the proposed dimer tool design), metal coordination has been shown to generate complexes suitable for crystallographic characterization. See, for example, S. L. Buchwald, R. T. Lum, and J. C. Dewan, *J. Am. Chem. Soc.* 108, 7441 **(1986)** and M. A. Bennett, J. A. Johnson, and A. C. Willis, *Organometallics* 15, 68 **(1996)**.

35. To calculate a transition energy between structures (**1**) and (**10**), the dimer and a π-bond (bond [1] in Fig. 4) were moved toward one another, maintaining parallelism but allowing optimization of both bond lengths, and of the rest of the structure. The resulting transition breaks two σ-bonds (at position [2] in Fig. 4) and encounters a high barrier (>0.4 aJ ≈ 60 kcal/mol).

36. R. Merkle, personal communication **(2004)**.

37. R. Smalley, *Sci. Am.* 76 **(2001)**.

38. In the intended application, DC10c tools would be reused, cycling repeatedly between the loaded and empty state. This might be accomplished by first binding ethene or ethyne to the tool, producing (**5**) or (**6**), then abstracting hydrogen atoms (using ethynyl radicals[19]) to produce (**1**). In the intended application environment, these molecules would occupy binding sites, and hence be presented to the empty tool in an oriented fashion that permits the application of force to overcome reaction barriers. Both of these cycloaddition reactions conserve orbital symmetry, and the strained π-bonded ring of DC10c would be expected to react much like a strongly activated diene; both the ethene and ethyne cycloadditions have strongly favorable reaction energies, −0.645 and −0.722 aJ, respectively. Abstraction of a pair of hydrogen atoms from (**5**) or (**6**) by a pair of alkynyl radicals has a favorable reaction energy per atom: −0.433 aJ for (**6**) → (**5**) and −0.223 for (**5**) → (**1**). The corresponding non-transfer probabilities are $\sim 10^{-46}$ and $\sim 10^{-24}$ at 300 K.

39. K. E. Drexler, Toward Integrated Nanosystems:Fundamental issues in design and modeling, in *Handbook of Computational and Theoretical Nanotechnology,* Michael Rieth and Wolfram Schommers, eds., American Scientific Publishers (in press).

40. W. Humphrey, A. Dalke, K. Schulten, *J. Mol. Graphics* 14, 33 **(1996)**.

41. A. A. Granovsky **(2005)**. Available at http://classic.chem.msu.su/gran/gamess/index.html

42. M. W. Schmidt, K. K. Baldridge, J. A. Boatz, S. T. Elbert, M. S. Gordon, J. H. Jensen, S. Koseki, N. Matsunaga, K. A. Nguyen, S. Su, T. L. Windus, M. Dupuis, and J. A. Montgomery, *J. Comput. Chem.* 14, 1347 **(1993)**.

Received: 31 January 2005. Accepted: 31 January 2005.